Magnetic Correlations in Short and Narrow Graphene Armchair Nanoribbons

Michael Golor,[1] Cornelie Koop,[1] Thomas C. Lang,[2] Stefan Wessel,[1] and Manuel J. Schmidt[1]

[1]*Institut für Theoretische Festkörperphysik, JARA-FIT and JARA-HPC, RWTH Aachen University, 52056 Aachen, Germany*
[2]*Department of Physics, Boston University, Boston, Massachusetts 02215, USA*
(Received 14 May 2013; published 21 August 2013)

Electronic states at the ends of a narrow armchair nanoribbon give rise to a pair of nonlocally entangled spins. We propose two experiments to probe these magnetic states, based on magnetometry and tunneling spectroscopy, in which correlation effects lead to a striking, nonlinear response to external magnetic fields. On the basis of low-energy theories that we derive here, it is remarkably simple to assess these nonlinear signatures for magnetic edge states. The effective theories are especially suitable in parameter regimes where other methods such as quantum Monte Carlo simulations are exceedingly difficult due to exponentially small energy scales. The armchair ribbon setup discussed here provides a promisingly well-controlled (both experimentally and theoretically) environment for studying the principles behind edge magnetism in graphene-based nanostructures.

Graphene [1], a two-dimensional network of carbon atoms, has induced much excitement among physicists because of a multitude of unusual electronic properties [2]. Much of the literature about graphene has focussed on noninteracting electrons moving on a honeycomb lattice, though. One reason for this is that free electrons already show unorthodox effects such as Klein tunneling [3,4] and an anomalous quantum Hall sequence even at room temperature [5]. Another reason is that the influence of short-ranged electron-electron interactions is considered to be weak because of the vanishing density of states at the charge-neutrality point [6].

At graphene edges the density of states may be peaked due to the presence of edge-localized states close to the Fermi level [8]. Especially at extended zigzag edges this leads to a phenomenon called edge magnetism, where various theories predict ferromagnetic intraedge and antiferromagnetic interedge correlations [9–18]. Experimentally, these magnetic correlation effects prove to be elusive. Only recently, experimental indications of the importance of electron-electron interactions at edges of chiral graphene nanoribbons have been reported [19]. The actual magnetic properties, however, remain unresolved experimentally as yet. The most severe issues hampering the experimental study of edge magnetism are (a) uncontrolled and rough edges [20], (b) hybridization with the substrate [21], and (c) unclear experimental signatures of edge magnetism. All these issues are in fact related to the high complexity of the edges of most graphene nanoribbons: On the one hand the exact structural properties of the ribbon edges are not known. On the other hand, theory has not yet provided clear experimentally resolvable signatures beyond mean-field band structures.

Here, we propose to study electronic correlation effects in a simpler geometry, namely in short armchair nanoribbons with zigzag ends (see Fig. 1). This geometry

resolves at least issues (a) and (c). The basic principles of edge magnetism become strikingly clear in those ribbons, since, compared to edge magnetism in large zigzag or chiral ribbons, they offer three key advantages: (i) suitable high-quality armchair ribbons are already available [22–24]; (ii) as we will show, armchair ribbons are well under control theoretically as they allow for essentially exact solutions without the need to resort to mean-field techniques; (iii) correlation effects are accessible by means of magnetometry and spin-resolved scanning tunneling spectroscopy (STS).

Model and geometry.—Our analysis is based on the π-band model of graphene. It is convenient for our purposes to separate the Hamiltonian $H = H_0 + H_U + H'$ into a dominant part

$$H_0 + H_U = -t \sum_{\langle i,j \rangle, \tau} c_{i\tau}^\dagger c_{j\tau} + U \sum_i c_{i\uparrow}^\dagger c_{i\uparrow} c_{i\downarrow}^\dagger c_{i\downarrow}, \quad (1)$$

where τ is a spin label, $t \approx 3$ eV is the nearest-neighbor hopping amplitude and $U \approx 6$ eV the on-site Hubbard repulsion. H' contains additional terms such as more distant neighbor hopping and the long-range part of the Coulomb repulsion. We will show that $H_0 + H_U$ governs the physics, while H' only renormalizes the effective parameters. The lattice geometry that we consider is characterized by the number of hexagons in the zigzag direction, W, and the number of hexagons in the armchair direction, L (see Fig. 1). High quality nanoribbons with $W = 3$ have recently been synthesized in a bottom-up approach in the laboratory [22–24]. They have been shown to be terminated by single hydrogen atoms [22], so that a π-band-only model is well justified.

Effective low-energy theory.—Following Ref. [25] we derive a fermionic theory for the low-energy sector of a $W = 3$ ribbon. The relevant degrees of freedom are selected on the basis of their localization properties. The eigenstates of H_0 are separated into bulk states $b_{\mu\tau}^\dagger = \sum_i \phi_\mu(i) c_{i\tau}^\dagger$ with
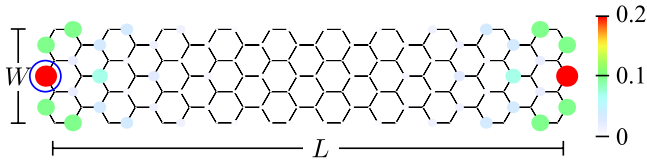
FIG. 1 (color online). Lattice geometry of an armchair nano-ribbon with $W = 3$ hexagons in zigzag direction and $L = 10$ hexagons in armchair direction. On top of the lattice the weight of the edge-localized low-energy states $|\psi_L(i)|^2 + |\psi_R(i)|^2$ is shown. Both the dot size and color scales with the weight. The blue circle indicates a typical site at which the spectral function is to be measured (see text).

$\sum_i |\phi_\mu(i)|^4 \sim 1/L$, and end states $e_{\pm\tau}^\dagger = \sum_i \psi_\pm(i) c_{i\tau}^\dagger$ with $\sum_i |\psi_\pm(i)|^4 \approx$ const for large L. The latter are symmetric and antisymmetric superpositions of exponentially localized states $e_{L/R,\tau}^\dagger$ at the left (L) and right (R) end of the ribbon. Typical end state wave functions are shown in Fig. 1. We reconstruct the states $e_{L/R,\tau}^\dagger$ from the low-energy eigenstates $e_{\pm,\tau}^\dagger$ of H_0. The energies of the end states $\epsilon_+ = -\epsilon_-$ are exponentially small in L while we find that the bulk energies for Eq. (1) satisfy $|\epsilon_\mu| \gtrsim 0.23t$. Thus, the end states are energetically well separated from the bulk states. From the end state wave functions $\psi_{L/R}(i)$ we construct a fermionic low-energy theory

$$H_f = -t^* \sum_\tau (e_{L\tau}^\dagger e_{R\tau} + \text{H.c.}) - \sum_{\tau,\tau',s=L,R} e_{s\tau}^\dagger (\mathbf{B} \cdot \boldsymbol{\sigma}/2)_{\tau\tau'} e_{s\tau'}$$
$$+ U^* \sum_{s=L,R} (e_{s\uparrow}^\dagger e_{s\uparrow} - 1/2)(e_{s\downarrow}^\dagger e_{s\downarrow} - 1/2), \quad (2)$$

where $t^* = |\epsilon_\pm|$ describes an effective hopping of electrons from one end to the other, $U^* = U \sum_i |\psi_L(i)|^4 = U \sum_i |\psi_R(i)|^4 \approx 0.1U$ is an effective Hubbard repulsion for the end-localized electrons, $\boldsymbol{\sigma}$ the vector of Pauli matrices, and $\mathbf{B}$ the magnetic field. We assume a g factor of 2. In Ref. [26] it was shown that the g factor can even be larger, so our estimates are conservative.

It is important to note, that U^* is essentially independent of L while t^* becomes exponentially small for large L. By fitting the numerical data we find $t^* \approx e^{-L/1.86} 1.29$ eV. Thus, for not too small L a further reduction of H_f to a two-spin Heisenberg model

$$H_H = J_H \mathbf{S}_L \cdot \mathbf{S}_R - \mathbf{B} \cdot (\mathbf{S}_L + \mathbf{S}_R), \quad J_H = 4(t^*)^2/U^* \quad (3)$$

is feasible. Here, $\mathbf{S}_{L/R}$ are spin-1/2 operators describing the spins of the localized electrons at the left/right end. This simple Heisenberg theory describes two antiferromagnetically coupled spins, localized at the ribbon ends, with a singlet-triplet (ST) splitting $J_H > 0$.

Assessing the effective theory.—In order to scrutinize the effective low-energy theories (2) and (3), we perform numerically exact projective auxiliary-field determinant quantum Monte Carlo (QMC) simulations of the full

lattice model $\tilde{H} = H_0 + H_U$. Ground-state averages of arbitrary observables $\hat{O}$, such as the energy or the Green's function, are calculated by $\langle \hat{O} \rangle = \langle \psi_T | e^{-\theta \tilde{H}} \hat{O} e^{-\theta \tilde{H}} | \psi_T \rangle / \langle \psi_T | e^{-2\theta \tilde{H}} | \psi_T \rangle$. The projection length $\theta = 120/t$ is chosen sufficiently large as to ensure convergence. $|\psi_T\rangle$ is taken as the ground state of the noninteracting system with a fixed number of spin-τ electrons N_τ. We employ a third-order Trotter-Suzuki decomposition with a propagation step size of $\Delta\tau = 0.01/t$. For further details on the QMC algorithm cf. Ref. [27].

Because of the SU(2) symmetry, the single scale in the low-energy sector is the ST splitting, J, which we calculate in three different ways. (i) In the fermionic theory we find $J_f = \sqrt{(U^*)^2/4 + 4(t^*)^2} - U^*/2$. (ii) In the Heisenberg theory J_H is given by Eq. (3). (iii) Within QMC simulations we calculate the difference J_{exact} of the total ground-state energies for $N_\uparrow = N_\downarrow + 2$ (triplet sector) and $N_\uparrow = N_\downarrow$ (singlet sector). Figure 2 compares these three results for $U/t = 0.5$ and 1.0. While J_f agrees very well with the exact solution, J_H deviates significantly for very short ribbons, where t^*/U^* is not yet small. Because of the exponentially small ST splitting, the QMC calculations were feasible only on relatively short ribbons $L \lesssim 8$. In this regime, the fermionic theory agrees with the exact QMC results within error bounds. The effective theory, however, is not restricted to such small L. We conclude from Fig. 2, that for $L \gtrsim 8$ the simple Heisenberg theory (3) may be used to describe the spin physics.

Detection via magnetometry.—The exponential dependence of J on L in combination with the discreteness of L enables an experimental detection of the interend spin correlation by means of magnetization measurements. Note that L must be even because of the synthesis process [24]. We assume an ensemble of $W = 3$ ribbons of variable and homogeneously distributed sizes $L = 8, 10, \ldots, 20$ (corresponding to lengths between 4 and 8 nm), arranged randomly and sparsely on a 2D surface. Other length
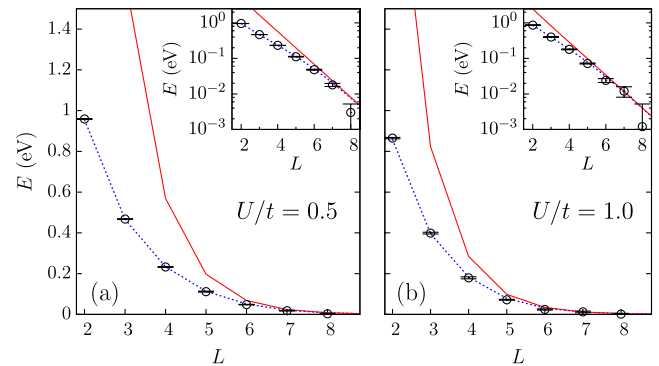

FIG. 2 (color online). Singlet-triplet splitting J as a function of ribbon length L. The blue dotted line is J_f calculated from H_f [Eq. (2)]. The red solid line corresponds to J_H [Eq. (3)]. The black circles with error bars are the results of the QMC simulations J_{exact}. (a) is with $U = 0.5t$ and (b) with $U = t$.

distributions can be accounted for easily. The surface of the largest ribbon is about 6 nm^2. Even if less than 1/10 of the substrate is covered by ribbons, 2×10^4 ribbons per μm^2 are possible. In Fig. 3 we show the total magnetic moment of an ensemble of 3000 ribbons for each length $L = 8, 10, \ldots, 20$. At low temperatures one can see a clear nonlinear response signature with steps of height 6000 μ_B. The spacing of the critical field strengths of the different steps corresponds roughly to 1 order of magnitude in the magnetic field. This nonlinear response signature is observable with cutting-edge experimental magnetometry techniques [28].

Spin-polarized STS.—A complementary method for detecting the spin correlations is spin-polarized STS, which measures the spin-resolved local spectral function

$$A_{i\tau}(\omega) = \frac{1}{Z} \sum_{m,n} |\langle m|c_{i\tau}^\dagger|n\rangle|^2$$
$$\times [e^{-\beta E_n} + e^{-\beta E_m}] \delta_\eta(\omega - (E_m - E_n)). \quad (4)$$

Here, $|n\rangle$ are manybody eigenstates of H with energy E_n. Although the usual definition of the spectral function involves Dirac delta functions, we use the Gaussian $\delta_\eta(x)$ with finite width η. This accounts for a finite experimental energy resolution of the spectral function due to finite lifetimes or due to the temperature of the electrons and holes tunneling from the STM tip into the system. Note that this temperature η is not necessarily equal to the ribbon temperature β^{-1} in a nonequilibrium situation. For i we choose a site at the ribbon edge, where one of the edge state wave functions is large (see Fig. 1). Here we opt for the site i on the left.

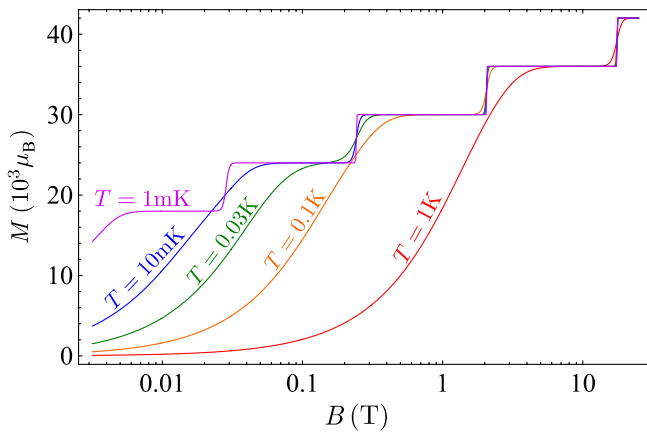The lattice electron operator $c_{i\tau}$ may be expressed in edge and bulk states. But since we are only interested in small energies ω we may drop the bulk states and obtain $A_{i\tau}(\omega) = |\psi_L(i)|^2 A_{L\tau}$, where $A_{L\tau}(\omega)$ is of the same form as Eq. (4), with the $c_{i\tau}$ operator replaced by $e_{L\tau}$. We have assumed that i is on the left end of the ribbon. We calculate the spectral function within the fermionic effective theory [Eq. (2)] by exact diagonalization. The resulting exact spectral function $A_{L\downarrow}(\omega)$ in dependence on the external magnetic field B is shown in Fig. 4. The large energy features provide a clear distinction between a singlet phase for $|B| < B_c$ and two triplet phases for $|B| > B_c$. For a better understanding of these large energy features we evaluate $A_{L\tau}(\omega)$ approximately for $U^* \gg B, T, t^*$ and find

$$A_{L\tau}(\omega) = \frac{1}{2} \sum_{\tau'} \delta_\eta\left(\omega + \tau'\frac{U^*}{2}\right) \frac{1 + e^{\beta J} + 2e^{2\tau\tau'\beta B}}{1 + e^{\beta J} + 2\cosh(2\beta B)}. \quad (5)$$

This approximate formula only holds for ω resolutions η coarser than the energy scales J, t^*. It shows that for $|B| < B_c = J/2$ it is possible to add a spin-down electron with energy $U^*/2$ and to remove a spin-down electron with energy $-U^*/2$, because the singlet phase is a coherent superposition of a state with an up spin and a state with a down spin on the left side. As $B > B_c = J/2$ the triplet state $e_{L\uparrow}^\dagger e_{R\uparrow}^\dagger|0\rangle$ becomes the ground state, where it is only possible to add a down spin electron but not to remove one. This is reflected by all the spectral weight being at positive ω. We also calculated the exact spectral function by QMC calculations (not shown in Fig. 4) and found that, within the statistical bounds achievable in QMC calculations, it agrees with Eq. (5) in the low-energy regime $|\omega| \lesssim U^*/2$.

In addition to the large energy features there is a subtle fine structure, shown in the insets of Fig. 4. Interestingly, the fine structure reflects all energy scales appearing in the effective theories, i.e., the interend hopping t^* and, on an
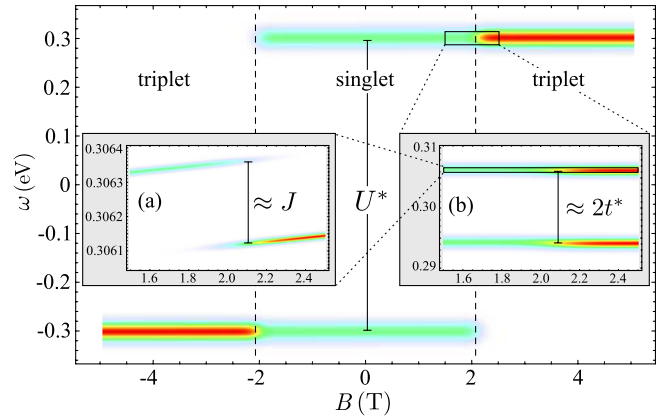

FIG. 3 (color online).   Total magnetic moment M (in 10^3 μ_B) of an ensemble of nanoribbons as a function of the magnetic field B for different temperatures. The ensemble contains 3000 ribbons for each length $L = 8, 10, \ldots, 20$. Each individual ribbon contributes two Bohr magnetons μ_B to the total moment if it is in the triplet state.

FIG. 4 (color online).   Spectral function $A_{L\downarrow}(\omega)$ for $t^* = 0.006\,$eV and $U^* = 0.6\,$eV, corresponding to a ribbon with $W = 3$ and $L = 10$. The critical field $B_c = \pm J/2 \approx 2.1\,$T is indicated by dashed lines. In the main plot the Gaussian smearing $\eta = 200$ Kelvin (see text). The insets show the fine structure of the spectral peaks with narrower Gaussian smearing of $\eta = 10$ Kelvin (b) and $\eta = 0.1$ Kelvin (a).

even finer level, the antiferromagnetic interedge coupling $J = 4(t^*)^2/U^*$. For different geometries, resulting in different effective model parameters, the energy scales of the fine structures scale accordingly.

Stability with respect to H'.—The fermionic low-energy theory [Eq. (2)] is derived by first order perturbation theory from $H_0 + H_U$, with the inverse bulk gap being the small parameter. As shown in Fig. 2, this is a remarkably good approximation. Moreover, due to overall SU(2) invariance, the low-energy spin physics must be governed by one single energy scale, namely the singlet-triplet splitting J. Thus it is reasonable to account for the additional terms H' in the effective Heisenberg model also in first order perturbation theory and calculate the corrections to J. We now discuss a variety of possible perturbation terms in H'. We find that the resulting corrections to J are smaller than the uncertainty for the literature parameters t and U.

In the special geometry discussed here, next-nearest neighbor hopping only gives rise to a shift in the chemical potential and may therefore be ignored. Third neighbor hopping and all other hoppings that couple the sublattices give contributions to t^* which are much smaller than the contribution of the nearest-neighbor hopping, since these more distant hoppings are exponentially suppressed as a function of distance. An electric field E along the ribbon gives rise to a correction $\Delta J = J(EL/2U^*)^2$.

Two additional terms arise from the long-range Coulomb interaction. On one hand there is the interedge term $V_{LR} n_L n_R$ with $n_s = \sum_\tau e_{s\tau}^\dagger e_{s\tau} - 1$, $V_{LR} \approx e^2 \exp(-L/L_{sc})/\kappa l$ with κ the dielectric constant and L_{sc} the screening length, both of which depend on the substrate. On the other hand there is an intraedge term $V_0 \sum_s (e_{s\uparrow}^\dagger e_{s\uparrow} - 1/2)(e_{s\downarrow}^\dagger e_{s\downarrow} - 1/2)$ with $V_0 \approx e^2 \sum_{i<j} |\psi_L(i)|^2 |\psi_L(j)|^2 \exp(-|\mathbf{r}_i - \mathbf{r}_j|/L_{sc})/\kappa|\mathbf{r}_i - \mathbf{r}_j|$, which has the same form as the Hubbard term in Eq. (2). Both terms contribute to the energy of the excited states with more or less than one electron at one end and therewith to U^*. Given the uncertainties for U in the literature (see, e.g., Ref. [29]), the actual value of the renormalized U^* with all corrections due to the environment is not accessible theoretically and needs to be determined experimentally. One way to do so is via a measurement of the spectral function (Fig. 4) in tunneling experiments. Crucially, however, the exponential length dependence of J is not spoiled by any of the perturbations to $H_0 + H_U$ discussed above.

Conclusion.—Motivated by the recent chemical synthesis of armchair ribbons with perfect zigzag ends [22–24], we have studied the magnetic correlations arising in these ribbons due to electronic interactions. We have identified spin-1/2 degrees of freedom at each end of the ribbon. This spin subsystem may be described by a simple Heisenberg model, which we have derived directly from a lattice model and benchmarked against numerically exact QMC simulations. The two end spins are coupled antiferromagnetically. The corresponding singlet-triplet splitting decays exponentially with the ribbon length. This enables

direct experimental access to the low-energy spin physics, for which we have proposed two complementary experiments. The setup proposed here thus allows us to study the basic principles of edge magnetism. A thorough understanding of this well-controlled scenario will facilitate the experimental investigation and the theoretical interpretation of edge magnetism in larger nanoribbons.

Note added.—Recently, we became aware of another theoretical investigation of armchair nanoribbons, focussing on their charge properties [30].

[1] K. S. Novoselov, A. K. Geim, S. V. Morozov, D. Jiang, Y. Zhang, S. V. Dubonos, I. V. Grigorieva, and A. A. Firsov, Science **306**, 666 (2004).

[2] N. M. R. Peres, Rev. Mod. Phys. **82**, 2673 (2010).

[3] A. F. Young and P. Kim, Nat. Phys. **5**, 222 (2009).

[4] C. W. J. Beenakker, Rev. Mod. Phys. **80**, 1337 (2008).

[5] K. S. Novoselov, Z. Jiang, Y. Zhang, S. Morozov, H. Stormer, U. Zeitler, J. Maan, G. Boebinger, P. Kim, and A. Geim, Science **315**, 1379 (2007).

[6] Note, however, that the long-range part of the Coulomb interaction gives rise to interesting renormalizations of the Dirac cone [7].

[7] V. N. Kotov, B. Uchoa, V. M. Pereira, F. Guinea, and A. H. Castro Neto, Rev. Mod. Phys. **84**, 1067 (2012).

[8] M. Fujita, K. Wakabayashi, K. Nakada, and K. Kusakabe, J. Phys. Soc. Jpn. **65**, 1920 (1996).

[9] J. Jung and A. H. MacDonald, Phys. Rev. B **79**, 235433 (2009).

[10] J. Jung, T. Pereg-Barnea, and A. H. MacDonald, Phys. Rev. Lett. **102**, 227205 (2009).

[11] Y.-W. Son, M. L. Cohen, and S. G. Louie, Phys. Rev. Lett. **97**, 216803 (2006).

[12] H. Karimi and I. Affleck, Phys. Rev. B **86**, 115446 (2012).

[13] Y.-W. Son, M. L. Cohen, and S. G. Louie, Nature (London) **444**, 347 (2006).

[14] T. Hikihara, X. Hu, H.-H. Lin, and C.-Y. Mou, Phys. Rev. B **68**, 035432 (2003).

[15] S. Dutta, S. Lakshmi, and S. K. Pati, Phys. Rev. B **77**, 073412 (2008).

[16] H. Feldner, Z. Y. Meng, A. Honecker, D. Cabra, S. Wessel, and F. F. Assaad, Phys. Rev. B **81**, 115416 (2010).

[17] H. Feldner, Z. Y. Meng, T. C. Lang, F. F. Assaad, S. Wessel, and A. Honecker, Phys. Rev. Lett. **106**, 226401 (2011).

[18] M. Golor, T. C. Lang, and S. Wessel, Phys. Rev. B **87**, 155441 (2013).

[19] C. Tao *et al.*, Nat. Phys. **7**, 616 (2011).

[20] J. Kunstmann, C. Özdoğan, A. Quandt, and H. Fehske, Phys. Rev. B **83**, 045414 (2011).

[21] Y. Li, W. Zhang, M. Morgenstern, and M. Mazzarello, Phys. Rev. Lett. **110**, 216804 (2013).

[22] L. Talirz *et al.*, J. Am. Chem. Soc. **135**, 2060 (2013).

[23] M. Koch, F. Ample, C. Joachim, and L. Grill, Nat. Nanotechnol. **7**, 713 (2012).

[24] J. van der Lit, M. P. Boneschanscher, D. Vanmaekelbergh, M. Ijäs, A. Uppstu, M. Ervasti, A. Harju, P. Liljeroth, and I. Swart, Nat. Commun. **4**, 2023 (2013).

[25] M. J. Schmidt, M. Golor, T. C. Lang, and S. Wessel, Phys. Rev. B **87**, 245431 (2013).

[26] A. V. Volkov, A. A. Shylau, and I. V. Zozoulenko, Phys. Rev. B **86**, 155440 (2012).

[27] F. F. Assaad and H. G. Evertz, Lect. Notes Phys. **739**, 277 (2008).

[28] H. Bluhm, N. C. Koshnick, J. A. Bert, M. E. Huber, and K. A. Moler, Phys. Rev. Lett. **102**, 136802 (2009).

[29] M. Schüler, M. Rösner, T. Wehling, A. Lichtenstein, and M. Katsnelson, Phys. Rev. Lett. **111**, 036601 (2013).

[30] M. Ijäs, M. Ervasti, A. Uppstu, P. Liljeroth, J. van der Lit, I. Swart, and A. Harju, arXiv:1306.2723.